ELSEVIER

Coordination Chemistry Reviews 230 (2002) 225–242

COORDINATION CHEMISTRY REVIEWS

www.elsevier.com/locate/ccr

Highlights of the spectroscopy, photochemistry and electrochemistry of [M(CO)$_4$(α-diimine)] complexes, M = Cr, Mo, W

Antonín Vlček, Jr. [a,b,*]

[a] *Department of Chemistry, Queen Mary and Westfield College, University of London, Mile End Road, London E1 4NS, UK*
[b] *J. Heyrovský Institute of Physical Chemistry, Academy of Sciences of the Czech Republic, Dolejškova 3, CZ-182 23 Prague, Czech Republic*

Received 9 October 2001; accepted 9 February 2002

Contents

Abstract

Tetracarbonyl-diimine complexes [M(CO)$_4$(α-diimine)] (M = Cr, Mo, W; α-diimine = polypyridyl (bpy, phen), pyridine-2-carbaldehyde (R-PyCa) or 1,4-diaza-butadiene, (R-DAB)) have very interesting structural, spectroscopic, electrochemical and photochemical properties. Their comprehensive experimental and theoretical investigations have important implications for our understanding of the chemistry of organometallic complexes with noninnocent ligands. The most interesting physical and chemical aspects of [M(CO)$_4$(α-diimine)] complexes, which have more general relevance, are highlighted and discussed.

Keywords: Spectroscopy; Photochemistry; Electrochemistry; [M(CO)$_4$(α-diimine)] complexes; MLCT

* Tel.: +44-20-78823260; fax: +44-20-78827794
E-mail address: a.vlcek@qmul.ac.uk (A. Vlček, Jr.).

0010-8545/02/$ - see front matter
PII: S0010-8545(02)00047-4

1. Introduction

Tetracarbonyl-diimine complexes [M(CO)$_4$(α-diimine)] of Group 6 transition metals (Cr, Mo, W) uniquely combine an electron-rich, low-valent d^6 metal atom, stabilized by four CO ligands, with an electron-accepting α-diimine ligand. This situation gives rise to a variety of intriguing spectroscopic, photochemical and electrochemical properties. [M(CO)$_4$(α-diimine)] complexes are well amenable to both experimental and theoretical studies. Over the past 40 years, or so, such investigations have significantly contributed to our understanding of electronic transitions and absorption spectra of organometallic compounds, structure and reactivity of their excited states, photochemical or electrochemical activation of a metal–carbonyl bond and of the properties of complexes with radical–anionic ligands, which are generated by electrochemical reduction. Because of their relative simplicity, [M(CO)$_4$(α-diimine)] complexes are excellent model systems to which new, state-of-the-art, experimental techniques and theoretical approaches are often applied at early stages of their development. Elaboration of resonance Raman spectroscopy as a tool for understanding the nature of electronic absorption, pressure- and excitation-wavelength dependent photochemistry, recognition of a bond-splitting reactivity of metal-to-ligand charge-transfer (MLCT) excited states and application of ultrafast time-resolved spectroscopy to characterize excited states and primary photoproducts are but a few examples. Recently, much information on the effects of electronic excitation and of one-electron reduction or oxidation have been obtained by combined electrochemical, spectroelectrochemical, spectroscopic and theoretical studies. By and large, investigations of the chemistry of [M(CO)$_4$(α-diimine)] complexes have wide implications for organometallic compounds containing noninnocent ligands. Rather general questions, such as localization of redox changes or electronic transitions on the metal atom and the ligands, structural effects of reduction, oxidation and electronic excitation, as well as photochemical or electrochemical means of bond activation have been addressed.

This review article is dedicated to Professor Derk J. Stufkens who had much contributed [1–12] to our understanding of spectroscopy and photochemistry of [M(CO)$_4$(α-diimine)] complexes and who later has broadly extended these studies to a wide range of photochemically and electrochemically active organometallic carbonyl–diimine complexes, including those with metal–alkyl or metal–metal bonds and α-diimine-substituted clusters [1,13–33]. The knowledge obtained through the studies on tetracarbonyl-diimine complexes has undoubtedly helped to understand the behavior of much more intricate organometallic molecules.

Hereafter, selected physical and chemical aspects of [M(CO)$_4$(α-diimine)] complexes (M = Cr, Mo, W), which have more general implications, will be highlighted and briefly discussed.

2. Slightly distorted pseudooctahedral structure

The schematic structure of [M(CO)$_4$(α-diimine)] complexes is shown in Fig. 1. In principle, these complexes can be regarded as being composed of two moieties, M(CO)$_4$ and the α-diimine ligand. [M(CO)$_4$(α-diimine)] complexes are known for a great variety of α-diimine ligands, ranging from polypyridines such as 2,2′-bipyridine or 1,10-phenanthroline to pyridine-2-carbaldehyde-imines (PyCa-R) and 1,4-diaza-1,3-butadiene (R-DAB), see Fig. 1. Besides that, various polyazine ligands (4,4′- or 2,2′-bipyrimidine, 2,2′-bipyrazine, 3,3′-bipyridazine, azo-2,2′-bipyridine, etc.) have been used, some of which form dinuclear complexes of the type [{M(CO)$_4$}$_2$(μ-polyazine)] [34–38].

[M(CO)$_4$(α-diimine)] complexes have a pseudooctahedral coordination geometry. Their spectroscopic properties can be interpreted within a C_{2v} symmetry. It is important to distinguish between axial and equatorial CO ligands which often manifest themselves differently in the spectra and show different reactivity. Optimization of the molecular geometry of [Cr(CO)$_4$(bpy)] [39], [M(CO)$_4$(phen)] (M = Cr, W) [40,41] or [W(CO)$_4$(*i*Pr-DAB)] [42] by DFT calculations shows that the axial C–M–C moiety is slightly bent away from the diimine ligand, 166–174°, in agreement with experimental values obtained [43–46] by X-ray diffraction for phen and R-DAB complexes: 163.1–172.4°. This axial bending is larger for R-DAB than bpy or phen complexes. It also affects IR and resonance Raman spectra [2,46,47]. The N–M–N bite angle is small, ca. 76°, while the equatorial C–M–C angle is close to 90°. Axial and equatorial CO ligands undergo rapid exchange, as was revealed by equilibration and ^{13}C-NMR studies of ^{13}CO-enriched DAB complexes [46,47].

3. Delocalized HOMO, predominantly α-diimine LUMO, σ–π* interaction and low-lying unoccupied π*-CO orbitals

Density functional theory (DFT) calculations of the electronic structure of [M(CO)$_4$(phen)] and [M(CO)$_4$-(tmp)] (M = Cr, W) [40,41], [Cr(CO)$_4$(bpy)] [39] and [W(CO)$_4$(*i*Pr-DAB)] [42] have revealed that the [M(CO)$_4$(α-diimine)] complexes have many common electronic features. A qualitative MO diagram is shown in Fig. 2.

The three highest occupied molecular orbitals a$_1$, a$_2$ and b$_1$ occur in an energetically narrow range, which is

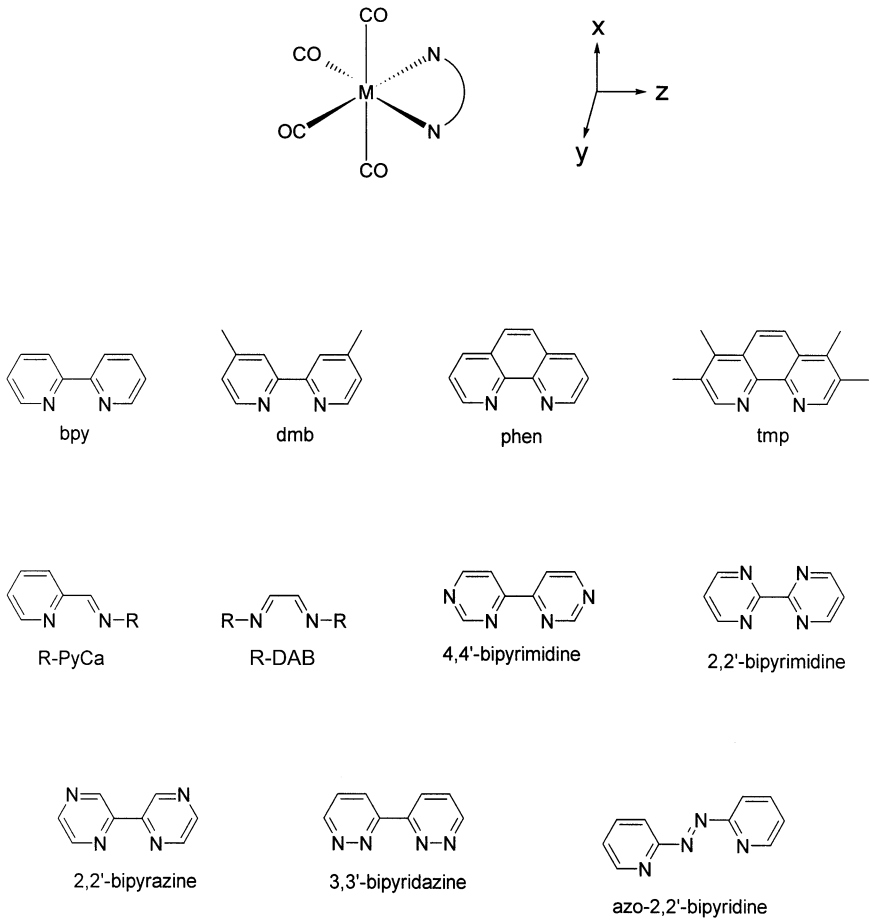

Fig. 1. Schematic structure of $[M(CO)_4(\alpha\text{-diimine})]$ complexes, chosen orientation of axes, and formulas of α-diimine ligands mentioned in the text. bpy = 2,2′-bipyridine, phen = 1,10-phenanthroline, dmb = 4,4′-dimethyl-2,2′-bipyridine, tmp = 3,4,7,8-tetramethyl-1,10-phenanthroline, PyCa = pyridine-2-carbaldehyde, DAB = 1,4-diaza-butadiene.

0.28–0.52 eV wide, depending on the particular complex. They decrease in energy in the order $a_1 > a_2 > b_1$.

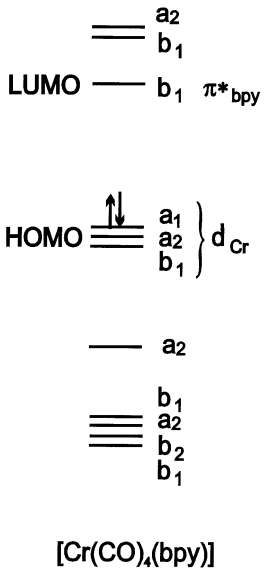

Fig. 2. MO diagram of $[M(CO)_4(\alpha\text{-diimine})]$ complexes, using $[Cr(CO)_4(bpy)]$ as a representative example [39].

All these orbitals are rather delocalized, containing between 43 and 63% of the metal d character and between 30 and 40% CO character. The b_1 HOMO-2 contains also a smaller α-diimine π* component. In particular, d_{z2}, together with a small d_{x2-y2} component contribute to the a_1 HOMO while the d_{yz} and d_{xz} orbitals participate in a_2 and b_1, respectively. The b_1 HOMO-2 is spectroscopically the most important mem-

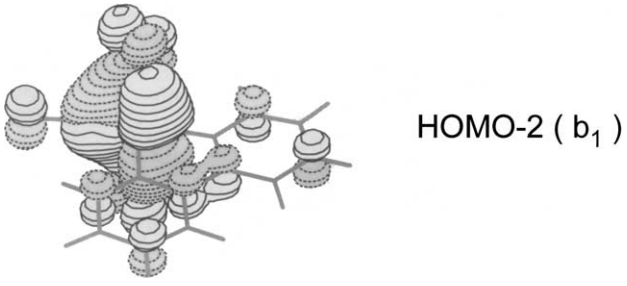

Fig. 3. The shape of the b_1 HOMO-2 of $[Cr(CO)_4(bpy)]$ calculated [39] by DFT using B3LYP functional. The HOMO-2 consists predominantly of the Cr $3d_{xz}$ orbital. Small π* CO and bpy contributions, which account for the Cr→CO and Cr→bpy π backbonding, respectively, can be seen.

ber of the HOMO manifold. Its shape, calculated for [Cr(CO)$_4$(bpy)], is shown in Fig. 3. On going from [W(CO)$_4$(phen)] to [W(CO)$_4$(*i*Pr-DAB)], the d_{xz} contribution in the b_1 HOMO decreases from 50 to 41% while the α-diimine π* participation increases concomitantly from 14 to 31%. The d_{xz}/π*(diimine) mixing in b_1 HOMO-2 describes the M→diimine π backbonding which generally strengthens in the order phen ~ bpy < R-PyCa < Ar-PyCa ~ R-DAB < Ar-DAB (Ar = aryl substituent such as *p*-tolyl, mesityl, *p*-anisyl, etc.). Orbitals of the axial CO ligands contribute to the b_1 HOMO-2 by ca. 18–22%. Interestingly, a small part (ca. 1.3% for [Cr(CO)$_4$(bpy)]) is due to an out-of-phase combination of σ-lone pairs of the two axial CO ligands. Equatorial CO ligands participate in the b_1 HOMO-2 by only 6–11%.

The LUMO of [M(CO)$_4$(α-diimine)] complexes has a b_1 symmetry, see Fig. 4. It is predominantly localized on the α-diimine ligand, as was manifested [39,41,42] by the DFT-calculated 68, 87 and 90% diimine paticipation in the b_1 LUMO of [W(CO)$_4$(*i*Pr-DAB)], [W(CO)$_4$(phen)] and [Cr(CO)$_4$(bpy)], respectively. The metal d_{xz} contribution varies between 1 and 10%, reflecting the M→diimine π backbonding. It is larger for R-DAB than phen and for W than Cr. The axial CO ligands participate in the b_1 LUMO through their π_z^* orbitals and the out-of-phase combination of the σ-lone pairs. These contributions were calculated for [Cr(CO)$_4$(bpy)] (3.4% total; 1.4% π and 2.0% σ) and [W(CO)$_4$(*i*Pr-DAB)] (1.4% total; 1.2% π and 0.2% σ). The σ–π* interaction within the b_1 LUMO has interesting spectroscopic and chemical consequences, which will be discussed later.

For complexes containing bpy or phen, the b_1 LUMO is followed in energy by a fully diimine-localized a_2 unoccupied orbital and, at somewhat higher energy, by another b_1 orbital of a predominantly diimine character. These two MOs are absent in R-DAB complexes. Importantly, a series of low-lying unoccupied π* CO orbitals occurs closely above these diimine-localized MO's. Its lowest member lies ca. 1.5 eV above the LUMO. It has a b_2 symmetry, being predominantly localized on axial CO's. It is closely followed in energy by $a_1(CO_{ax})$, $b_2(CO_{eq})$ and $b_1(CO_{eq})$ molecular orbitals. The presence of the energetically low-lying π*(CO) orbitals in [M(CO)$_4$(α-diimine)] has important spectroscopic and photochemical implications, vide infra.

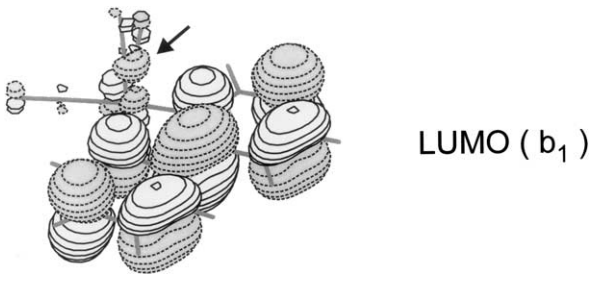

Fig. 4. The shape of the b_1 LUMO of [Cr(CO)$_4$(bpy)] calculated [39] by DFT using the B3LYP functional. The LUMO is mostly localized at the bpy ligand, with a small Cr $3d_{xz}$ contribution. The arrow indicates the σ contribution from axial CO ligands, which accounts for the σ–π* delocalization, see the text.

4. Single oxidation and several successive reduction steps

[M(CO)$_4$(α-diimine)] complexes are electrochemically reduced in several successive steps and oxidized in a single one-electron step. The first one-electron reduction is both electrochemically and chemically reversible, producing the corresponding radical-anions [M(CO)$_4$(α-diimine)]$^{\bullet -}$ [35,37,38,41,48–50]. The first reduction potential depends strongly on the diimine ligand while the metal atom has a much smaller influence. For example, the first reduction of [M(CO)$_4$(bpy)] occurs at −1.84, −1.91 and −1.99 V versus Fc^+/Fc for M = W, Mo and Cr, respectively [49]. The second one-electron reduction of bpy or phen complexes, which occurs ca. 0.6 V more negatively, is chemically irreversible due to a fast dissociation of a CO ligand. Pentacoordinated [M(CO)$_3$(α-diimine)]$^{2-}$ species, which presumably contain a highly π-delocalized M(α-diimine)$^{2-}$ moiety, are formed [51]. A third reduction was found for phen complexes at potentials 0.5 V more negative still. It is a complicated process which involves consumption of two to three electrons [51]. Electrocatalytic reduction of the supporting electrolyte may be involved. On the other hand, [M(CO)$_4$(4,4′-Ph$_2$-bpy)] complexes show four successive reversible one-electron reduction steps that are not accompanied by a CO loss, at least at low temperatures [49]. This behavior arises from the large redox capacity of the 4,4′-Ph$_2$-bpy ligand which has two low-lying unoccupied orbitals [49].

Oxidation of [M(CO)$_4$(α-diimine)] complexes occurs in a single one-electron step, which is chemically irreversible for M = Mo and W [40,52]. In contrast, phen, tmp, 2,2′-bipyrazine or 3,3′-bipyridazine complexes of chromium are oxidized reversibly [35,37,40]. The oxidation product $[Cr(CO)_4(tmp)]^+$ has been characterized spectroelectrochemically at low temperatures [40].

5. Reduction products [M(CO)$_4$(α-diimine)]$^{\bullet -}$ contain a radical–anionic α-diimine$^{\bullet -}$ ligand

The first one-electron reduction is localized predominantly at the diimine ligand. This conclusion is supported by several observations: (i) [M(CO)$_4$(α-diimine)] complexes show the same reduction pattern (number of steps, number of electrons exchanged) as the free α-diimine ligand itself. Compared with the free ligands, the

first reduction of the corresponding complexes is shifted positively by about 0.5–0.8 V. The positive shift on coordination is even larger when a polyazine ligand bridges between two metal atoms [35,38] in complexes of the type [{$M(CO)_4$}$_2$(μ-polyazine)]. (ii) Reduction potentials of the [$M(CO)_4$(α-diimine)] complexes correlate with reduction potentials of the free diimine [37,38,41,49]. (iii) Although the first reduction potential slightly increases on going from Cr to Mo and W [35,41,49,50], the metal has a much smaller effect than the diimine ligand. (iv) EPR spectra of the reduced [$M(CO)_4$(α-diimine)]$^{\bullet -}$ complexes and of their dinuclear counterparts [{$M(CO)_4$}$_2$(μ-polyazine)]$^{\bullet -}$ show spectroscopic features characteristic of the corresponding diimine$^{\bullet -}$ radical-anions, such as large ^{14}N EPR hyperfine splitting constants and hyperfine interaction with the diimine protons [34,36,39,41,48,50,53–56]. (v) A broad, structured absorption band in the red or NIR spectral region (above 600 nm) and a strong, sharp band between 360 and 390 nm are observed in the UV–Vis spectra of [$M(CO)_4$(α-diimine)]$^{\bullet -}$. Both these spectral features are diagnostic for the presence of an α-diimine$^{\bullet -}$ chromophore [49,53,54,57]. The conclusion that the one-electron reduction of [$M(CO)_4$(α-diimine)] complexes is predominantly localized at the diimine ligand is supported by DFT calculations on [$Cr(CO)_4$(bpy)]$^{0/\bullet -}$ [39] and [$M(CO)_4$(N,N)]$^{0/\bullet -}$ (M = Cr, W, N,N = phen, tmp) [41]. For example, it was calculated that 76% of the electron density increase accompanying the reduction of [$Cr(CO)_4$(bpy)] to [$Cr(CO)_4$(bpy)]$^{\bullet -}$ is localized at the bpy ligand, while the charge on the Cr atom remains nearly unchanged [39].

From the historical point of view, it is interesting to note that early studies of [$M(CO)_4$(α-diimine)] reduction helped to decide the question whether α-diimines and other noninnocent ligands in highly reduced complexes stabilize unusually low metal oxidation states by strong π backbonding or whether they are reduced themselves, producing complexes of metals in common oxidation states with radical–anionic ligands [48]. This old question of coordination chemistry was clearly decided in favor of the latter answer since the [$M(CO)_4$(α-diimine)]$^{\bullet -}$ species behave spectroscopically as complexes of zero-valent d^6 metal atoms Cr, Mo or W with a radical–anionic diimine$^{\bullet -}$ ligand.

6. LUMO symmetry switching between phenanthroline and tetramethyl–phenanthroline complexes have profound spectroelectrochemical effects

Comparison between [$M(CO)_4$(phen)] and [$M(CO)_4$(tmp)] complexes provides a nice example how subtle structural changes of the diimine ligand affect the properties of reduced [$M(CO)_4$(α-diimine)]$^{\bullet -}$ radical anions [41]. The LUMOs of [$M(CO)_4$(phen)] and [$M(CO)_4$(tmp)] are predominantly diimine-localized but have different symmetry, b_1 and a_2, respectively. This LUMO symmetry switching occurs also between the free phen and tmp ligands [58]. This difference has hardly any effect on the structure and properties of the parent complexes. The first reduction potential shows a small negative shift on going from phen to tmp. Characteristically, the W complexes are reduced more positively than the Cr ones: −2.04 V (Cr/phen), −2.24 V (Cr/tmp), −1.87 V (W/phen), and −2.09 V (W/tmp), measured in *n*PrCN versus Fc/Fc$^+$. (Data from ref. [41]; the earlier published value for [$Cr(CO)_4$(tmp)] is corrected herein.) In contrast to the nearly identical properties of the neutral species, the EPR spectra of the radical–anions are profoundly different: [$M(CO)_4$(phen)]$^{\bullet -}$ complexes show large hyperfine splitting from the ^{14}N donor atoms and from the pairs of ^{1}H atoms at C3,8 and C4,7 positions. On the other hand, EPR spectra of [$M(CO)_4$(tmp)]$^{\bullet -}$ show large hyperfine splitting from ^{1}H atoms of a pair of CH_3 groups at C4,7 positions and two pairs of ^{1}H atoms at C2,9 and C5,6, while the ^{14}N-splitting is rather small. Reasonable agreement between experimental and DFT-calculated hyperfine splitting was obtained. It follows that these differences reflect the different distributions of the b_1 and a_2 LUMOs over the phen and tmp ligands, respectively, and manifest the predominant ligand-localization of the first reduction of [$M(CO)_4$(α-diimine)] complexes [41].

7. Diimine-localized reduction is accompanied by increasing π backdonation to equatorial CO ligands and σ–π* delocalization over the axial OC–M–CO moiety

Above, it was shown that reduced [$M(CO)_4$(α-diimine)]$^{\bullet -}$ complexes can be regarded as containing diimine$^{\bullet -}$ radical–anionic ligand coordinated to a d^6 M(0) metal atom. However, the actual picture is not that simple since the ligand reduction has a profound influence on the electron density distribution within the $M(CO)_4$ fragment. This is clearly manifested by the shifts of the A_1^2, B_1, A_1^1 and B_2 ν(CO) IR bands of [$Cr(CO)_4$(bpy)] to lower frequencies upon reduction by −18, −26, −36 and −35 cm^{-1}, respectively [55]. A detailed IR spectroelectrochemical study of ^{13}CO-enriched [$Cr(CO)_4$(bpy)] has determined that the axial and equatorial CO stretching force constants decrease on reduction by 21 and 68 Nm^{-1}, respectively [55]. This experiment shows that the reduction is accompanied by a strong drift of electron density toward equatorial CO ligands through increasing π backbonding. The π* electron density increase on the axial CO ligands is much smaller. The EPR spectrum of the ^{13}CO-enriched [$Cr(CO)_4$(bpy)]$^{\bullet -}$ shows the typical bpy$^{\bullet -}$ pattern,

small hyperfine splitting from the ^{53}Cr nucleus (0.128 mT) and, importantly, hyperfine splitting from the ^{13}C nuclei of the axial ^{13}CO ligands, $a(^{13}C_{ax}) = 0.601$ mT. No hyperfine interaction with the ^{13}C nuclei of equatorial ^{13}CO ligands was observed [55]. The EPR spectrum thus indicates that the spin density is delocalized from bpy$^{\bullet -}$ to the axial CO ligands only, seemingly in contradiction with the IR spectroelectrochemical results discussed above. This puzzle was solved by a DFT theoretical study [39] of the [Cr(CO)$_4$(bpy)] reduction. It was found that ca. 75% of the extra electron density in [Cr(CO)$_4$(bpy)]$^{\bullet -}$ resides on the bpy ligand, 24% on the four CO ligands and only 0.8% on the Cr atom. Importantly, DFT calculations have demonstrated that delocalization of the extra electron density in [Cr(CO)$_4$(bpy)]$^{\bullet -}$ over the two equatorial CO ligands (14.2%) is much larger than over the two axial CO ligands (9.6%), in agreement with IR spectroelectrochemistry. DFT calculations have also confirmed that most of the spin density is localized on the bpy$^{\bullet -}$ ligand, while small, but nearly equal, amounts of 0.0066 and 0.0063 reside on the axial and equatorial C(CO) atoms, respectively. It follows that the experimentally observed ^{13}C(CO) hyperfine splitting is not determined by the total amount of spin density at the ^{13}C atoms, but, instead, by the mechanism of spin delocalization. The electron (spin) density from bpy$^{\bullet -}$ is delocalized over equatorial CO ligands only through the participation of the $\pi_x^*(CO_{eq})$ orbitals in the SOMO, see Fig. 4. The spin density at the equatorial ^{13}C nuclei is negligible since they lie in the nodal plane of the b_1 SOMO, rendering the EPR hyperfine splitting too small to be observed. The electron (spin) delocalization over the axial CO ligands follows a very different mechanism. Orbitals of each axial CO contribute to the SOMO by 1.4%. Part of this contribution is due to an involvement of the $\pi_z^*(CO_{ax})$ orbitals in the SOMO, which does not give rise to any appreciable ^{13}C hyperfine splitting. In addition, a σ–π* interaction between the σ-lone pairs of the axial CO ligands and the singly occupied bpy$^{\bullet -}$ π* orbital occurs within the SOMO, as was described in Part 3 above. This σ-contribution has a large 2s(C) component, whose involvement in the SOMO increases the spin density at the axial C nuclei, leading to a significant ^{13}C hyperfine splitting. These different mechanisms of spin delocalization over axial and equatorial ligands is manifested both by the experimentally observed ^{13}C(CO) splitting constants (0.601 mT, ∼0 mT, respectively) and by Fermi contact terms calculated for the ^{13}C nuclei of the axial and equatorial ^{13}C(CO) atoms: 5.627×10^{-4} and 0.037×10^{-4} cm^{-1}, respectively [39]. In conclusion, it follows that the EPR hyperfine splitting from donor atoms of ancillary ligands of transition metal complexes with radical–anionic ligands does not reflect the total delocalization of the spin density but, instead, its mechanism. The so called, σ/π* polarization or σ–π* hyperconjugation [59,60] has been often invoked to explain the hyperfine splitting from the donor atoms of axial ancillary ligands (e.g. ^{31}PR$_3$) in complexes with radical–anionic ligands such as [M(PR$_3$)(CO)$_3$(diimine$^{\bullet -}$)] (M = Cr, Mo, W) [48,50,59], [M(PR$_3$)$_n$(CO)$_{4-n}$(*o*-semiquinone)] (M = Re, Mn) [59,61] and others [59]. The combined experimental and theoretical study [39,55] of the [Cr(CO)$_4$(bpy)] reduction has revealed a detailed picture of this effect.

Theoretical analysis of the electron density distribution in [Cr(CO)$_4$(bpy)] and [Cr(CO)$_4$(bpy)]$^{\bullet -}$ has also shown that it is not sufficient to discuss electronic effects of reduction only in terms of the redox orbital, that is the b_1 LUMO of [Cr(CO)$_4$(bpy)], which becomes the SOMO in [Cr(CO)$_4$(bpy)]$^{\bullet -}$. It was calculated [39] that the extra electron density is much more delocalized than the b_1 SOMO itself, which is localized from 93.7% at the bpy ligand, 1.9% at Cr, 2.8% at the two axial CO ligands and 1.6% at both equatorial CO ligands. This SOMO distribution contrasts with the calculated increase of Mulliken population on these fragments: 75.6% (bpy), 0.8% (Cr), 9.6% (2CO$_{ax}$) and 14.2% (2CO$_{eq}$). It follows that the electron density redistribution upon reduction is determined by two effects: (i) delocalization of the b_1 LUMO redox orbital and (ii) compensating changes in the lower-lying occupied orbitals that are not directly involved in the reduction process. In the particular case of [Cr(CO)$_4$(bpy)], the electron density in the low-lying orbitals shifts toward the CO ligands, compensating for the increased electron donation from the bpy$^{\bullet -}$ ligand to the Cr atom and diminished Cr → bpy π backbonding.

8. Diimine-localized reduction activates an axial M–CO bond

Electrolytic reduction of [M(CO)$_4$(bpy)] in the presence of PPh$_3$ leads to a selective formation of *fac*-[M(PPh$_3$)(CO)$_3$(bpy)] via an electrode-catalyzed process [50]:

$$[M(CO)_4(bpy)] \overset{+e^-}{\rightleftarrows} [M(CO)_4(bpy)]^{\bullet -} \quad (1)$$

$$[M(CO)_4(bpy)]^{\bullet -} + PPh_3 \rightarrow \textit{fac}\text{-}[M(PPh_3)(CO)_3(bpy)]^{\bullet -} + CO \quad (2)$$

$$\textit{fac}\text{-}[M(PPh_3)(CO)_3(bpy)]^{\bullet -} \overset{-e^-}{\rightleftarrows} \textit{fac}\text{-}[M(PPh_3)(CO)_3(bpy)] \quad (3)$$

$$\textit{fac}\text{-}[M(PPh_3)(CO)_3(bpy)]^{\bullet -} + [M(CO)_4(bpy)] \rightarrow \textit{fac}\text{-}[M(PPh_3)(CO)_3(bpy)] + [M(CO)_4(bpy)]^{\bullet -} \quad (4)$$

The selective substitution of an axial CO ligand in [M(CO)$_4$(bpy)]$^{\bullet -}$ by PPh$_3$ (eq. 2) is the crucial step. Its rate constant and, hence, the labilization of an axial M–CO bond decrease in the order Cr > Mo > W [50]. The

σ–π* interaction, discussed in Sections 3 and 7 above, may contribute to this effect.

9. Redistribution of electron density upon oxidation of [Cr(CO)$_4$(tmp)] keeps the charge on the Cr atom nearly constant despite its oxidation to d^5 Cr(I)

Chemically and electrochemically reversible oxidation was observed for several [Cr(CO)$_4$(α-diimine)] complexes, where α-diimine is phen, tmp or bidiazine [35,37,40]. A comprehensive IR, EPR and UV–Vis spectroelectrochemical and DFT-computational study [40] has revealed that oxidation of [Cr(CO)$_4$(tmp)] is predominantly Cr-localized. The Cr atom in the oxidation product [Cr(CO)$_4$(tmp)]$^{\bullet+}$ has a d^5 electron configuration which implies a formal Cr oxidation state I. The d^5 electron configuration is clearly manifested [40] by the $g_{\|}$–$g_{\perp}$ anisotropy of 0.1, that is typical for metal-centered radicals [62]. In agreement, the SOMO of [Cr(CO)$_4$(tmp)]$^{\bullet+}$ was calculated [40] to have between 57 and 72% 3d Cr character. Despite this change in electron configuration from d^6 to d^5 upon oxidation, the overall Mulliken electron population on the Cr atom decreases by only 0.061 e$^-$. It follows that the Cr-centered oxidation of [Cr(CO)$_4$(tmp)] is accompanied by a compensating shift of electron density from the four CO ligands (−0.633 e$^-$) and, to a lesser extent, the tmp ligand (−0.306 e$^-$). The extensive weakening of the Cr→CO π backdonation upon oxidation is manifested by the dramatic changes in the IR spectrum that accompany oxidation of [Cr(CO)$_4$(tmp)] to [Cr(CO)$_4$(tmp)]$^{\bullet+}$, see Fig. 5: The ν(CO) bands shift by nearly 100 cm^{-1} to higher wavenumbers while the three lower ν(CO) bands corresponding to the out-of-phase A_1^1, B_1 and B_2 modes, collapse into a single, broad IR band. The upward shift clearly demonstrates the decrease of Cr→CO π backdonation, while the close proximity of the wavenumbers of A_1^1, B_1 and B_2 vibrational modes shows that the axial and equatorial CO stretching force constants become nearly equal and the ax–eq interaction force constant increases upon oxidation [40].

Oxidation of [M(CO)$_4$(diimine)] complexes labilizes M–CO bonds. Cyclic voltammetry indicates that the reactivity of oxidized phen, tmp and bpy complexes increases in the order Cr < Mo < W. Oxidatively-induced substitution of a CO ligand by a solvent molecule was observed for [Mo(CO)$_4$(bpy)] and its kinetics and mechanism were studied electrochemically [52]. Cr complexes appear to undergo relatively slow complete loss of all CO ligands upon oxidation [40].

10. Low-lying MLCT electronic transitions

All [M(CO)$_4$(α-diimine)] complexes are strongly colored due to a well-developed absorption band in the visible spectral region [63,64]. Based on its high intensity ($\varepsilon \cong 4000$–$10\,000$ M^{-1} cm^{-1}), this band was attributed to a M→diimine MLCT transition. This assignment is supported by the fact that such a band is absent in the spectra of the complexes [M(CO)$_4$(diamine)], where the diamine ligand does not have any low-lying orbitals, capable of accepting an electron upon excitation, diamine = ethylenediamine (en) [63,65,66], propylenediamine [63], *N*,*N*,*N*′-trimethylethylenediamine [63] or *N*,*N*,*N*′,*N*′-tetramethylethylenediamine [9].

Electronic transitions in [M(CO)$_4$(α-diimine)] complexes were the subject of several theoretical studies. [Cr(CO)$_4$(bpy)] and [Cr(CO)$_4$(H-DAB)] were calculated by CASSCF/CASPT2 [67,68] while TD-DFT was applied to [W(CO)$_4$(*i*Pr-DAB)] [42], [M(CO)$_4$(phen)] and [M(CO)$_4$(tmp)]; M = Cr, W [41,69]. These calculations revealed that the principal electronic transition responsible for the visible absorption band occurs from the a^1A_1 ground state to an $^1A_1$ excited state (b^1A_1 for diimine = R-DAB or bpy; c^1A_1 for phen or tmp). b_1(HOMO-2)→b_1 π*(diimine) is the principal (ca. 90%) orbital excitation contributing to this transition, regardless whether the b_1 π*(diimine) orbital is the LUMO (diimine = R-DAB, bpy, phen) or LUMO+1 (diimine = tmp), see Figs. 3 and 4 and Section 3 for the orbital description. It follows that the lowest allowed transition involves charge transfer from the metal and axial CO orbitals to the π*(diimine) orbital. The calculated changes of electron density distribution on the individual molecular fragments upon $a^1A_1 \rightarrow b^1A_1$ excitation of [Cr(CO)$_4$(bpy)] fully support the description of this transition as MLCT: the Mulliken electron population on Cr, each axial CO and each equatorial CO ligand decreases by 0.36, 0.13 and 0.08 e$^-$, respectively, accompanied by an increase of 0.79 e$^-$ at the bpy ligand [39]. It is interesting to note that the electron density on the bpy ligand increases by about the same amounts upon MLCT excitation and one-electron reduction of [Cr(CO)$_4$(bpy)] [39]. Several other M→diimine MLCT transitions were calculated to lie in the energy range of the visible absorption band. However, due to their very low intensities, they contribute only to the broadening of the band and to its low-energy tail.

The strong visible absorption band is followed in energy by a relatively weak band at around 400 nm, that is present even in the spectra of [M(CO)$_4$(en)] and related complexes [63–65]. Traditionally, it was assigned to a LF transition arising from excitation between d orbitals. However, more recent theoretical [41,42,68,69] as well as experimental [42] research shows convincingly that it originates in low-lying M→CO MLCT transitions. The much stronger absorption that occurs deeper

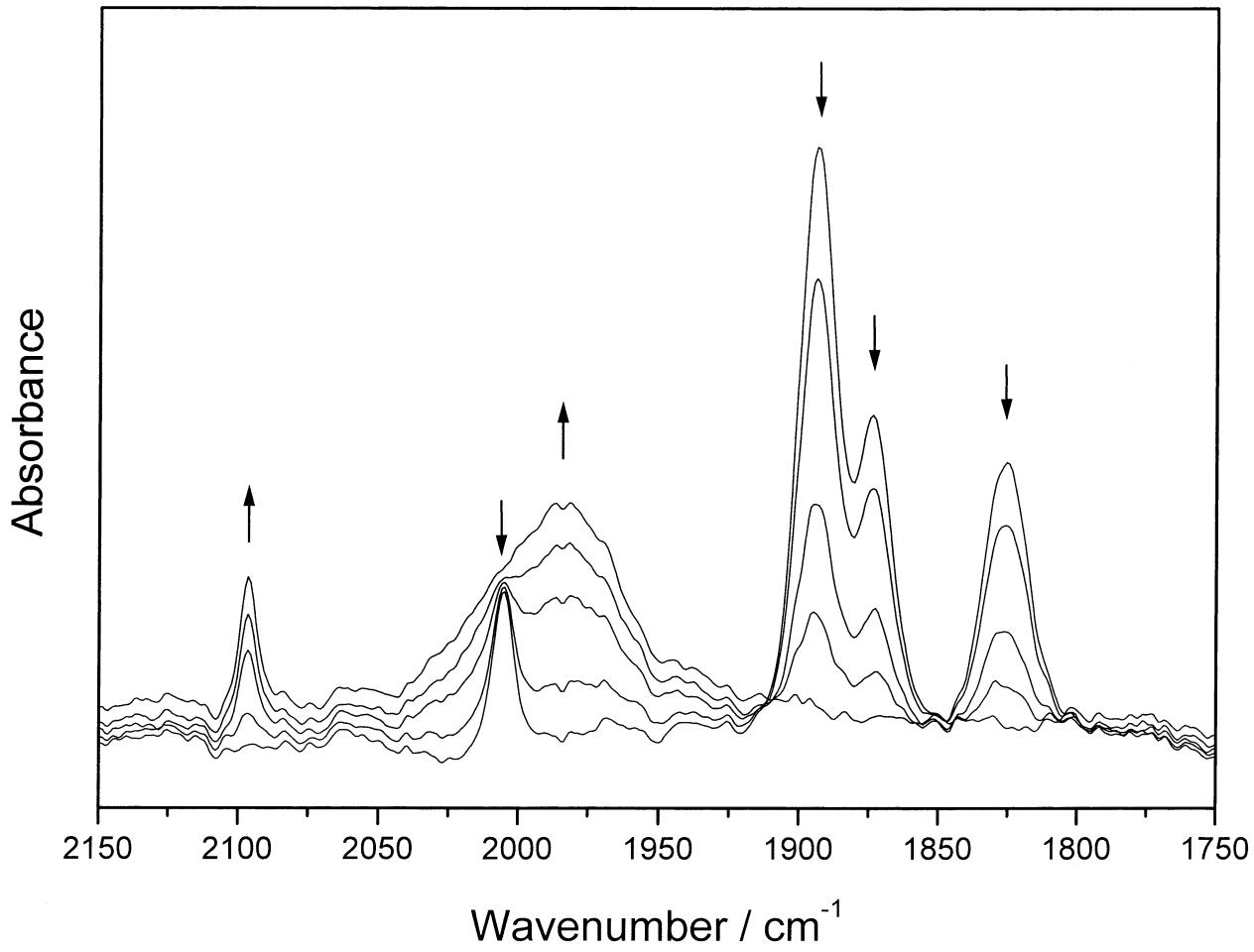

Fig. 5. IR spectra monitored during the course of electrochemical oxidation of $[Cr(CO)_4(tmp)]$ in *n*PrCN solution in an optically transparent thin layer electrochemical cell at 193 K [40]. Arrows show bands of $[Cr(CO)_4(tmp)]$ (↓) and of the oxidation product $[Cr(CO)_4(tmp)]^+$ (↑).

in the UV region is due to higher M→CO and M→diimine MLCT transitions.

11. Solvatochromism reflects the amount of charge transferred upon MLCT excitation

$[M(CO)_4(\alpha\text{-diimine})]$ complexes show a negative solvatochromism which manifests itself by a shift of the intense visible MLCT absorption band to higher energies (i.e. shorter wavelengths) as the solvent polarity increases. The solvatochromic shift often exceeds 100 nm and is clearly observable as a color change from blue/violet to orange [1,3–7,9,64,70–74]. The MLCT band also slightly shifts to higher energies upon increasing the external pressure [72] or decreasing the temperature [5,72], due to a pressure- or temperature-dependence of the solvent polarity [72]. The solvatochromism of the MLCT transition of the $[M(CO)_4(\alpha\text{-diimine})]$ complexes is usually interpreted by different stabilization of the ground and excited states by electrostatic (mainly dipole–dipole) interactions with polar solvents [1,64,71,73–75]. Generally, the $[M(CO)_4(\alpha\text{-diimine})]$ molecules are more polar in their electronic ground state than the MLCT excited state due to a diimine→M σ donation, which leads to a $M^{\delta-}(\alpha\text{-diimine}^{\delta+})$ charge distribution in the ground state. M→diimine MLCT excitation transfers negative charge from M to the diimine, decreasing the molecular dipole moment. The energy difference between the ground and excited states is larger in more polar solvents which more strongly stabilize the polar ground state relative to the MLCT excited state. The solvatochromism correlates with the dipole-moment change upon excitation and measurements of the solvatochromic shift serve as a qualitative indication of the amount of electron density actually transferred on MLCT transition. This will be large for complexes with weak M→diimine π back-bonding in which the mixing between the d_{xz} and π*(diimine) orbitals is small and the b_1(HOMO-2)→b_1(LUMO) transition has a predominantly charge transfer character. On the other hand, the polarity change will be small in complexes with a highly π delocalized M(diimine) chelate ring, where the

b_1(HOMO-2) and b_1(LUMO) are predominantly π bonding and π antibonding, respectively, to the M–N bonds [1]. Hence, solvatochromism qualitatively correlates with the charge-transfer character of the electronic transition, the extent of M→diimine π backbonding and π delocalization within the M(diimine) chelate ring. Solvatochromism of [M(CO)$_4$(α-diimine)] complexes decreases as a function of the diimine ligand in the order: phen ≅ bpy > R-PyCa > Ar-PyCa ≫ R-DAB ≫ Ar-DAB [5,6,9,72]. The notion of solvatochromism as an experimental probe of the nature of electronic transitions is now widely used in organometallic spectroscopy to study not only absorption bands due to MLCT but also ligand-to-ligand and sigma-bond-to-ligand charge transfer transitions [1,15–31].

12. Resonance Raman spectra probe the character of the lowest allowed electronic transition

Depending on the extent of the M→diimine π backbonding, Raman spectra measured in resonance or preresonance with the lowest allowed electronic transition of [M(CO)$_4$(α-diimine)] show two patterns which gradually change into each other as a function of the diimine ligand or, to a lesser extent, the metal atom. Herein, they will be called 'MLCT' and 'delocalized', respectively, according to the character of the resonant electronic transition. The 'MLCT resonance Raman pattern' consists of a strongly enhanced band due to the higher (in-phase) ν(CO) A_1^2 vibration (typically at 2000–2010 cm^{-1}) and a group of high-frequency intra-diimine vibrations. Their number depends on the diimine ligand. For example, bpy, phen or tmp complexes typically show three strong bands between 1400 and 1650 cm^{-1} and a few weaker bands between 1000 and 1350 cm^{-1} [6,9,11,12,41,42]. The diimine region of resonance Raman spectra of complexes of the much simpler R-DAB ligand is dominated by a single strongly enhanced ν(CN) band at around 1500 cm^{-1} [6,33,42]. Low-frequency (< 800 cm^{-1}) deformation and M–C stretching skeletal vibrations are occasionally observed in the 'MLCT Raman pattern', but only with weak intensities [6,9,11,41,42]. The 'MLCT pattern' is typical for complexes with weak M→diimine π backbonding, whereby the b_1(HOMO-2) and b_1(LUMO) are localized predominantly on the M(CO)$_4$ fragment and π* diimine, respectively. The $b_1(d_{xz},CO)\rightarrow b_1$(diimine) excitation then affects the C≡O bonds and the C=N bonds within the diimine ligand, giving rise to a strong resonance enhancement of the Raman bands due to modes which involve ν(CO) and ν(CN) vibrations [1].

The selective enhancement of the Raman band due to the higher A_1^2 ν(CO) mode is a remarkable feature of resonance Raman spectra of [M(CO)$_4$(α-diimine)] complexes [1,3–6,12,33]. The intensity of the A_1^2 ν(CO) Raman band provides an indication of the charge transfer character of the resonant electronic transition [1,6,33]. Enhancement of the A_1^2 ν(CO) Raman band is a direct evidence for the electron-density redistribution within the M(CO)$_4$ fragment upon MLCT excitation, which affects the strength and length of the C≡O bonds, see Section 10. The A_1^2 ν(CO) mode corresponds to an in-phase combination of axial and equatorial C≡O stretching vibrations. Hence, distortions of axial and equatorial C≡O bonds upon MLCT excitation sum up and both contribute to the overall excited state distortion along the corresponding normal coordinate, giving rise to a strong resonance Raman effect [11,76]. In contrast, the lower A_1^1 mode corresponds to an out-of-phase combination of axial and equatorial C≡O stretching vibrations and the respective bond distortions upon excitation nearly cancel out. Therefore, the overall distortion of the A_1^1 normal coordinate on excitation is too small to produce an observable resonance Raman effect [11,76].

The second, 'delocalized resonance Raman pattern' is typical for [M(CO)$_4$(α-diimine)] complexes with strong M→diimine π backbonding. In this case, the b_1(HOMO-2)→b_1(LUMO) excitation involved in the resonant MLCT transition occurs between orbitals which are largely delocalized over the M(diimine) chelate ring, having a M–N π and π* character, respectively. Hence, the ν(CO) band is enhanced only very weakly, if at all. (For example, no ν(CO) band was observed in the resonance Raman spectrum of [W(CO)$_4$(*p*-tol-DAB)] [6].) Below ca. 1600 cm^{-1}, a whole series of resonantly enhanced bands due to vibrations of the diimine ligand appears, while deformation vibrations of the M(diimine) chelate ring, ν(MN) and ν(MC) vibrations occur below ca. 800 cm^{-1} with significant intensities [4,6,7,12]. It follows that the structural effects of delocalized π→π* excitation of the M(diimine) chelate ring is distributed over many normal coordinates.

At its extreme, the 'MLCT resonance Raman pattern' is typical for bpy and phen complexes. However, its features are prevalent also for complexes of R-PyCa, Ar-PyCa and R-DAB. Fully developed 'delocalized pattern' was observed for complexes containing Ar-DAB ligands. In general, the typical 'MLCT' Raman features become less prominent while the delocalized features emerge as a function of the diimine ligand on going from bpy or phen to R-PyCa, Ar-PyCa, R-DAB and, especially, to Ar-DAB [1,3–7,9]. A similar trend was observed as the metal changes from Cr to Mo and W [6]. The change of 'MLCT' into 'delocalized' resonance Raman pattern with changing the metal or diimine ligand is usually accompanied by a decrease of solvatochromism [6], since both effects reflect the MLCT character of the lowest allowed transition.

The dependence of resonance Raman band intensities on the excitation wavelength has revealed [41] that the lowest allowed electronic transitions of $[W(CO)_4(phen)]$ and $[W(CO)_4(tmp)]$ have the same principal component $b_1(HOMO\text{-}2) \rightarrow b_1(\pi^*)$, whether the $b_1(\pi^*)$ orbital is the LUMO (phen) or not (tmp). In the case of the binuclear complex $[\{M(CO)_4\}_2(\mu\text{-}2,2'\text{-bipyrimidine})]$, resonance Raman spectra measured with different excitation wavelengths were used to distinguish between absorption bands due to excitations into different 2,2′-bipyrimidine π^* orbitals [10].

Resonance Raman criteria for characterizing allowed electronic transitions, that were much developed by the Amsterdam group [1–7,9–12] using $[M(CO)_4(\alpha\text{-diimine})]$ complexes and analogous $[Fe(CO)_3(R\text{-DAB})]$ [14], are now widely applied to a broad range of organometallic diimine metal complexes and diimine-substituted metal clusters [1,15–32]. Effects of metal–ligand interaction on resonance Raman spectra of a series of *i*Pr-DAB complexes have been analyzed with the aid of DFT calculations and are discussed in detail in a review article [33].

13. Photophysics: multiple emission

$[M(CO)_4(\alpha\text{-diimine})]$ complexes (α-diimine = bpy or phen and their derivatives) show two emission bands in fluid solutions or low-temperature glasses [1,9,65,69,70,77]. These bands are usually called high-energy (HE) and low-energy (LE). They occur around 530 and 670 nm, respectively, in a 80 K glass. Emission of Cr complexes is very weak and short-lived. Hence, most of the data were obtained on Mo and W complexes. Excitation spectra of the LE emission correspond to the absorption spectra [65]. Emission lifetime measurements [65,69] have revealed that the LE emission band results from a radiative decay of two excited states. For example, lifetimes of 150 an 490 ns were observed for $[W(CO)_4(phen)]$ in a 2-Me-THF glass at 80 K [69]. These two states become equilibrated in a fluid solution, decaying with common, ca. 27 ns, lifetime [65] or shorter [69]. The LE band shows the solvatochromism and rigidiochromism typical for emission from M → diimine MLCT states [9,65,69,70]. Based on these experimental criteria, as well as on TD-DFT calculations of triplet electronic transitions [69], the LE emission has been attributed to a radiative decay of two M → diimine MLCT states, presumably $^3A_1$ and a slightly lower-lying $^3B_2$. These two states arise predominantly from $b_1(d_{xz}$ HOMO-2) → $b_1(\pi^*$-phen LUMO) and $a_2(d_{yz}$ HOMO-1) → $b_1(\pi^*$-phen LUMO) triplet excitations, respectively.

In accordance with the emission studies, two excited states of a W → phen MLCT character, with a ca. 5 ns lifetime, have been observed in picosecond time-resolved visible absorption spectra of $[W(CO)_4(phen)]$ [78]. The M → diimine MLCT character of the lowest excited state of $[W(CO)_4(\alpha\text{-diimine})]$; α-diimine = bpy, dmb, *i*Pr-PyCa; has been confirmed by excited-state resonance Raman spectroscopy [79] which have shown the typical upward shift of the A_1^2 ν(CO) band by some 50 cm^{-1} and bands corresponding to a reduced α-diimine$^{\bullet -}$ ligand. Similarly, femtosecond time-resolved visible absorption spectrum of $[Cr(CO)_4(bpy)]$ shows the presence of two excited states with 8 and 87 ps lifetimes [80], whose Cr → bpy MLCT character was confirmed by picosecond time-resolved IR spectra [81,82].

The HE emission band is fully developed only in the spectra measured with excitation into higher UV absorption bands [65,69]. Excitation spectrum of the HE emission of $[W(CO)_4(4\text{-Me-phen})]$ shows a single band at ca. 350 nm. A small shift of the HE emission band to higher energies with decreasing excitation wavelength [9,65] indicates that it originates in several radiative transitions. HE emission of $[W(CO)_4(phen)]$ and $[W(CO)_4(tmp)]$ decays with a very short lifetime, < 40 ns at 80 K [69]. Based on triplet TD-DFT calculations performed on $[W(CO)_4(phen)]$ and $[W(CO)_4(tmp)]$, it was concluded [69] that the HE emission originates in low-lying W → CO MLCT excited states, in contrast to the traditional LF assignment.

To summarize, $[M(CO)_4(\alpha\text{-diimine})]$ complexes (α-diimine = bpy and phen derivatives) show two low-lying emissions from M → diimine MLCT states and a higher-lying emission from M → CO MLCT state(s). The two former states are equilibrated in fluid solutions but not in 80 K glasses. The M → diimine and M → CO MLCT states are not in equilibrium, regardless of the temperature.

The emission spectroscopic pattern shows an interesting dependence on the diimine ligand which was studied [9] for $[W(CO)_4(\alpha\text{-diimine})]$; diimine = 4,7-$Ph_2$-phen, *i*Pr-PyCa, *i*Pr-DAB [1,9]. Whereas $[W(CO)_4(4,7\text{-}Ph_2\text{-phen})]$ shows both LE and HE emission bands in benzene solution at 298 K, the LE band is completely absent in the solution spectra of $[W(CO)_4(i\text{Pr-PyCa})]$ and $[W(CO)_4(i\text{Pr-DAB})]$. Similarly, in a 2-Me-THF glass at 80 K, the intensity of the LE band relative to the HE band sharply decreases on changing the diimine from 4,7-Ph_2-phen to *i*Pr-PyCa. The LE emission disappears completely for $[W(CO)_4(i\text{Pr-DAB})]$. This diimine-dependence of the intensity of the LE emission parallels the decreasing solvatochromism and the changing resonance Raman spectral pattern from 'MLCT' to partly 'delocalized', see Sections 11 and 12 above. This sharp decrease of the LE emission intensity on going from phen to R-PyCa and, especially, R-DAB was explained by the change of the character of the emissive state from W → diimine MLCT to essentially ππ* of the delocalized W(*i*Pr-DAB) unit, which accelerates the rate of a nonradiative decay. This is caused by the involve-

ment of low-frequency skeletal vibrations which provide better coupling between the delocalized excited state and the ground state [1,9]. Activation of skeletal vibrations is clearly manifested by the 'delocalized resonance Raman pattern', see Section 12.

14. Photochemical CO substitution follows dissociative and associative pathways, depending on experimental conditions

[M(CO)$_4$(α-diimine)] complexes undergo a photochemical substitution of an axial CO ligand:

$$[M(CO)_4(\alpha\text{-diimine})] \overset{h\nu,+L}{\rightarrow} fac\text{-}[M(CO)_3(L)(\alpha\text{-diimine})] + CO \quad (5)$$

where L is a solvent molecule or a nucleophile such as phosphine, phosphite, nitrile, pyridine, etc. Quantum yield of CO photosubstitution shows complex and interrelated dependences on the metal atom [6,70,83–85], diimine ligand [6,8,70], irradiation wavelength [70,78,83–89], pressure [83–85,87], temperature [70,86], solvent [78,86], and, for Mo and W, also on the type and concentration of the entering ligand L [8,78,84,85,87].

The main features of [M(CO)$_4$(α-diimine)] photosubstitution have been revealed by a detailed analysis of all these dependences:

a) The photosubstitution quantum yield ϕ decreases in the order Cr ≫ Mo > W.

b) The photosubstitution quantum yield ϕ sharply decreases on changing the irradiation wavelength from UV to visible spectral region.

c) The photosubstitution quantum yield ϕ of [Cr(CO)$_4$(α-diimine)] decreases as a function of diimine in the order phen > bpy > *i*Pr-Pyca > *i*Pr-DAB > Ph-PyCa > *p*tol-DAB [6]. Similar, but less pronounced dependence was observed for Mo complexes [6].

d) Photochemical CO substitution in [M(CO)$_4$(phen)] (M = Mo, W) complexes follows parallel dissociative and associative pathways, described by equations 6 and 7, respectively.

Dissociative photosubstitution:

$$[M(CO)_4(\alpha\text{-diimine})] \overset{h\nu,Solv}{\rightarrow} fac\text{-}[M(CO)_3(Solv)(\alpha\text{-diimine})] + CO \quad (6a)$$

$$fac\text{-}[M(CO)_3(Solv)(\alpha\text{-diimine})] \overset{+L}{\rightarrow} fac\text{-}[M(CO)_3(L)(\alpha\text{-diimine})] \quad (6b)$$

Associative photosubstitution:

$$[M(CO)_4(\alpha\text{-diimine})] \overset{h\nu,+L}{\rightarrow} *[M(\cdots L)(CO)_4(\alpha\text{-diimine})] \quad (7a)$$

$$*[M(\cdots L)(CO)_4(\alpha\text{-diimine})] \rightarrow fac\text{-}[M(CO)_3(L)(\alpha\text{-diimine})] + CO \quad (7b)$$

where * denotes the excited state.

The photosubstitution quantum yield can be expressed [84,85] by eq. 8 as a sum of quantum yields of the dissociative and associative pathways, denoted ϕ_d and ϕ_a, respectively. The quantum yield of the associative pathway ϕ_a is proportional to the concentration of the entering nucleophile L:

$$\phi = \phi_d + \phi_a = \phi_d + k_a[L] \quad (8)$$

e) The associative contribution k_a determined for [M(CO)$_4$(phen)] complexes decreases on going from W to Mo [84,85]. The CO photosubstitution of [Cr(CO)$_4$(phen)] [83,84,87] and [Cr(CO)$_4$(bpy)] [86] is entirely dissociative.

f) The associative contribution k_a determined for [M(CO)$_4$(phen)] (M = Mo, W) complexes increases with increasing nucleophilicity and decreasing cone angle of the phosphine ligand L [8,84,85]. The cone angle is more important for Mo than W, while the nucleophilicity is the most important factor for W. For example, the relative importance of the associative pathway in the case of [Mo(CO)$_4$(phen)] under visible-light irradiation decreases in the order $PMe_3 > PBu_3 \gg PPh_3$. The associative pathway prevails over the dissociative one for PMe_3 and PBu_3, while the reaction with PPh_3 is predominantly dissociative. In contrast, CO photosubstitution in [W(CO)$_4$(phen)] is predominantly associative even for PPh_3.

g) The associative contribution k_a determined for [M(CO)$_4$(phen)] (M = Mo, W) complexes increases with increasing external pressure [83–85,87].

h) The associative contribution k_a determined for [Mo(CO)$_4$(phen)] increases with increasing the

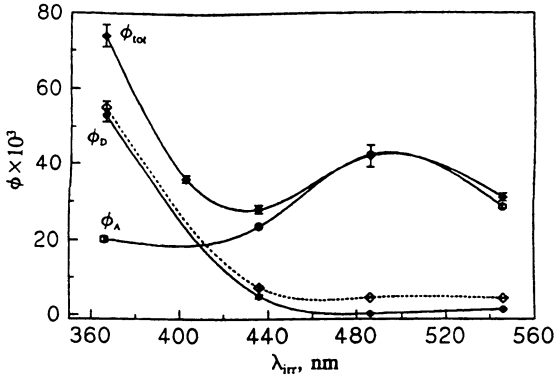

Fig. 6. Quantum yield of photochemical CO substitution in [Mo(CO)$_4$(phen)] by PMe_3 [84]. ϕ_{tot} (◆) = total quantum yield, ϕ_D = quantum yield of the dissociative pathway, ϕ_A = quantum yield of the associative pathway. All data measured using [PMe_3] = 0.0506 M. ϕ_{tot} (----) = total quantum yield measured using [PMe_3] = 0.0051 M.

irradiation wavelength from 366 to 436 nm and, even more, to 486 nm, followed by a small decrease on going to 546 nm [84]. It should be noted that k_a is substantial even under UV irradiation at 366 nm, see Fig. 6.

i) Quantum yield of the dissociative pathway ϕ_d, determined for [Mo(CO)$_4$(phen)] and [W(CO)$_4$(phen)] [84,85], decreases sharply on changing the irradiation wavelength from UV to the visible spectral region, where it becomes very small and apparently constant, see Fig. 6.

j) The different irradiation-wavelength dependences of k_a and ϕ_d give rise to an unusual increase in the overall quantum yield ϕ with increasing the irradiation wavelength in the visible spectral region for reactions which have a large associative component. This behavior was observed when [Mo(CO)$_4$(phen)] [84] or [W(CO)$_4$(phen)] [78] was irradiated in the presence of PBu_3 in high concentrations, Fig. 6.

k) The total quantum yield of the dissociative CO substitution from [Cr(CO)$_4$(bpy)] [86] and [Cr(CO)$_4$(phen)] [83,87] is substantial (10^{-2}–10^{-1}) even under irradiation in the visible spectral region, where it shows a pronounced dependence on the irradiation wavelength. This behavior will be discussed in Section 16 below.

l) The photosubstitution quantum yield ϕ of [W(CO)$_4$(cyclo-Pr-DAB)] measured using irradiation into the W→DAB MLCT absorption band is very small and nearly independent of the chemical nature of L [8], indicating that the associative pathway (7) is not important for DAB complexes. Indeed, a detailed study [89] of the photochemistry of [Mo(CO)$_4$(*i*Pr-DAB)] in low-temperature matrices has demonstrated that dissociation of the axial CO ligand is the primary photochemical step. The dissociative mechanism of CO substitution in [M(CO)$_4$(*i*Pr-DAB)] (M = Mo, W) by olefins in alkane solutions was established by quantum-yield and time-resolved spectroscopic measurements [89]. The latter have identified [M(solv)-(CO)$_3$(*i*Pr-DAB)], which is the key intermediate of the dissociative mechanism (6). The quantum yield of the dissociative substitution of CO in [W(CO)$_4$(*i*Pr-DAB)] by (*E*)-cyclooctene was found [89] to decrease with increasing irradiation wavelength: 0.092 (254 nm), 0.080 (302 nm), 0.038 (365 nm), 0.019 (405 nm) and ~0.001 (548 nm). Nearly identical values were obtained for [Mo(CO)$_4$(*i*Pr-DAB)]. The very low value measured at 548 nm is independent of the cyclooctene concentration and of the metal, Mo or W. It can be concluded that the lowest M→DAB MLCT excited state of [M(CO)$_4$(R-DAB)] (M = Mo, W) undergoes only a very inefficient axial CO dissociation [89].

In short, irradiation of [Cr(CO)$_4$(α-diimine)] complexes with UV or visible light leads to CO dissociation that is accompanied by solvent coordination. The quantum yield sharply decreases on changing the diimine ligand from bpy or phen to PyCa and to DAB ligands. Photochemical CO substitution of [Mo(CO)$_4$(phen)] and [W(CO)$_4$(phen)] complexes follows parallel dissociative and associative pathways. Generally, the dissociative pathway is predominant under UV irradiation while the associative mechanism prevails under irradiation with visible light. The associative pathway is especially important for CO photosubstitution in [W(CO)$_4$(phen)] by highly nucleophilic, small phosphine molecules such as PBu_3 or PMe_3. It is accelerated by increasing the phosphine concentration and external pressure. Photosubstitution of Mo and W complexes containing other phen- and bpy-type ligands follow the same mechanism as described above for the phen complexes. In contrast, DAB and, presumably, also PyCa complexes appear to undergo only a dissociative CO substitution, whose efficiency drops sharply on changing the irradiation wavelength from UV to the visible spectral region.

15. Photochemical M–CO dissociation occurs from M→diimine and M→CO MLCT excited states

Photochemical CO substitution in [M(CO)$_4$(α-diimine)]; M = Cr, Mo, W; complexes involves independent reactions from at least two different electronic excited states that are populated by near-UV and visible irradiation, respectively (see Fig. 7). This is clearly manifested by the sharp quantum yield decrease on changing the irradiation wavelength from near-UV to the visible. Further evidence is provided by profoundly different quantum yield dependences on the temperature [86] and pressure [83–85,87] observed under near-UV and visible irradiation.

According to a traditional model of organometallic photochemistry [90], the dissociative CO photosubstitution (6) was assigned to LF states while the associative pathway (7) was attributed to the lowest-lying M→diimine MLCT states. However, results of recent theoretical, spectroscopic and photochemical studies indicate that this model needs to be modified, especially with respect to the role of the LF states [91].

There is now a mounting evidence that UV irradiation leads to CO dissociation from M→CO MLCT excited states, instead of LF states. Any direct photochemical role of LF excited states is very unlikely in view of recent theoretical calculations on [Cr(CO)$_4$(bpy)] [67,68], [W(CO)$_4$(phen)] and [W(CO)$_4$(tmp)] [69] and on [W(CO)$_4$(*i*Pr-DAB)] [42] which clearly show that the singlet and triplet LF excited states lie too high in energy to be excited by near-UV or visible irradiation or to be

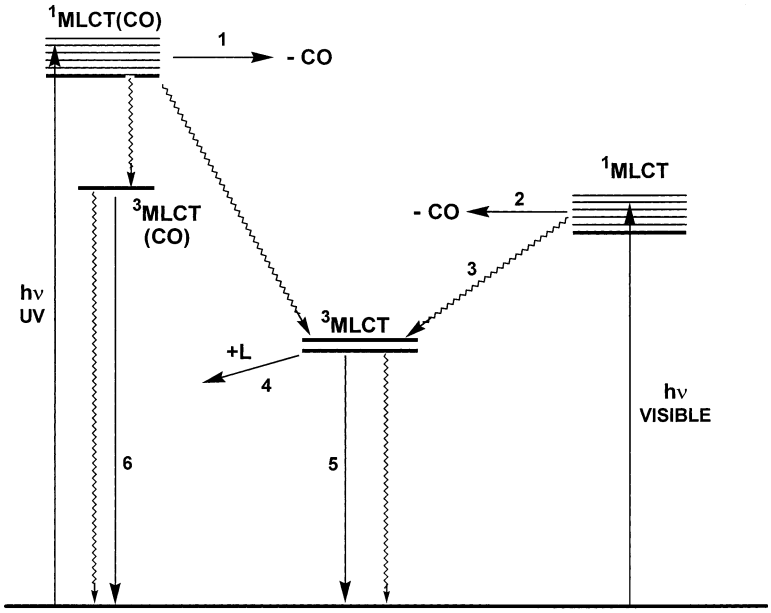

Fig. 7. Excited state (Jablonski) diagram of $[M(CO)_4(\alpha\text{-diimine})]$ complexes. 1: Ultrafast CO dissociation from M→CO MLCT excited state under UV irradiation. 2: Ultrafast CO dissociation from $^1A_1$ M→diimine MLCT excited state under visible irradiation occurs in parallel with relaxation into non-dissociative ^{3}MLCT states, 3. (This is the branching of the evolution of the lowest optically prepared $^1A_1$ MLCT excited states between the reaction 2 and relaxation 3, as explained in the text.) 4: Associative CO substitution by an incoming nucleophile or oxidation by MV^{2+}. This reaction is possible only for complexes with sufficiently long-lived ^{3}MLCT states, i.e. for M = Mo, W, diimine = phen, bpy, not DAB. 5: LE emission. 6: HE emission.

thermally back-populated from low-lying M→diimine MLCT excited states. However, a manifold of M→CO MLCT transitions have been calculated to occur closely above the lowest M→diimine MLCT states. Moreover, both theoretical and spectroscopic evidence [42] show that M→CO MLCT transitions are responsible for the weak absorption band at around 400 nm, which is ubiquitous in the absorption spectra of $[M(CO)_4(\alpha\text{-diimine})]$ complexes, see Section 10. At the same time, CO dissociation from upper M→diimine MLCT states, which can also be populated by near-UV excitation, seems unlikely, because their potential energy surfaces were calculated [68] to have a quasibound shape. These considerations indicate that near-UV irradiation of $[M(CO)_4(\alpha\text{-diimine})]$ complexes populates low-lying M→CO MLCT excited states from which facile CO dissociation takes place.

Contrary to the traditional interpretation, the optically prepared M→diimine ^{1}MLCT excited state was found to be directly involved in the axial-CO dissociation from $[M(CO)_4(\alpha\text{-diimine})]$ complexes under visible-light irradiation. This conclusion is supported by the following evidence: (i) For $[Cr(CO)_4(\alpha\text{-diimine})]$, it was observed that the quantum yield of CO dissociation and the resonance enhancement of the A_1^2 ν(CO) Raman band, which is a unique property of the allowed MLCT transition, show a qualitatively identical dependence on the diimine ligand: phen > bpy > *i*Pr-Pyca > *i*Pr-DAB > Ph-PyCa > *p*-tol-DAB [6,12]. (ii) CO dissociation from $[Cr(CO)_4(bpy)]$ is an ultrafast reaction which occurs in less than 400 fs [80–82,86,92], in parallel with population of two ^{3}MLCT excited states, whose photochemical role was excluded by an observation of their rapid (8 and 87 ps) and quantitative decay to the ground state [80–82]. (iii) The potential energy curves calculated for the three lowest-lying Cr→bpy ^{1}MLCT excited states are nearly unbound [68]. Time-dependent calculation of the wave-packet propagation on the potential energy surface of the b^1A_1 Cr→bpy ^{1}MLCT excited state predicts [68] the axial CO dissociation to be completed in less than 500 fs after visible-light excitation, in accord with experiments [80–82].

Theoretical CASSCF/MR-CCI calculations [68] also revealed the origin of the seemingly counterintuitive unbound character of the lowest Cr→bpy MLCT states in $[Cr(CO)_4(bpy)]$: The energies of the, initially very high-lying, ^{1}LF excited states, that are derived from $3d\rightarrow 3d_{x2}$ excitations, decrease rapidly along the reaction coordinate, as the axial Cr–CO distance increases. A strongly avoided crossing with the ^{1}MLCT states occurs and modifies the shape of the lower MLCT energy surface, making it nearly unbound along the axial Cr–CO coordinate, see Fig. 8. The MLCT excited state acquires some LF character as the Cr–CO distance increases. On an orbital level, it is possible to view this process as a mixing between $b_1(\pi^*\text{-bpy})$ and $3d_{x2}$

orbitals. A small energy barrier emerges due to the avoided state crossing. Its presence was confirmed by the observation that the quantum yield is temperature-dependent with apparent activation energies of 1349 and 1426 cm^{-1}, measured using 497 and 557 nm irradiation, respectively [86]. It should be noted that the energy difference between the interacting LF and MLCT states remains large everywhere along the reaction coordinate and, hence, the two states never really cross. The CO dissociation from the low-lying MLCT excited state can be viewed [93] as an adiabatic evolution on the potential energy surface of the optically prepared b^1A_1 excited state, whose character gradually changes from purely Cr→bpy MLCT to partially mixed MLCT/LF. An essentially equivalent description of this process [94] invokes a vibronic coupling between MLCT and LF states through an asymmetric axial C–Cr–C stretching vibration, whose activation leads to dissociation of an axial CO ligand.

The observed decrease of the quantum yield of CO dissociation from $[M(CO)_4(phen)]$ complexes in the order Cr ≫ Mo > W [83–85] results from several factors. Firstly, the efficiency of competitive intersystem crossing into low-lying, nondissociative ^{3}MLCT excited states is expected to increase in the same order because of increasing spin-orbit coupling. Secondly, the interaction between MLCT and LF states in the avoided crossing region weakens in the order Cr > Mo > W due to increasing MLCT-LF energy separation. Thirdly, the range of the stabilizing M-CO π interaction increases in the order Cr < Mo < W, because 5d orbitals and, to a lesser extent, 4d orbitals are much more diffuse than Cr 3d orbitals. Hence, the M–CO bond energy is less sensitive to the M–CO distance for W and Mo than Cr and the MLCT-LF avoided crossing occurs later on the reaction coordinate and with higher energy barrier for W and Mo than Cr.

The associative photochemical CO substitution of W and Mo complexes involves a direct interaction between the entering nucleophile L and electronically excited $[M(CO)_4(\alpha\text{-diimine})]$ complexes. It was attributed to low-lying ^{3}MLCT excited states which are sufficiently long-lived to allow for a bimolecular interaction. Moreover, the formally oxidized Mo or W atom in a MLCT-excited complex $*[M^+(CO)_4(\alpha\text{-diimine}^-)]$ is highly electrophilic, capable of interacting with the incoming nucleophile. This picture is compatible with the experimental results summarized above in Section 14: The associative photochemistry of Mo and W phenanthroline complexes is favored by relatively long nanosecond lifetimes of their ^{3}MLCT states [65,69,78], as well as by the large size of the Mo and W atoms. Both these factors make the associative pathway unfavorable for Cr complexes: the ^{3}MLCT states have lifetimes shorter than 100 ps [80] and the Cr atom is considerably smaller than Mo or W. Interestingly, similar changeover from a mixed associative/dissociative mechanism to purely dissociative on going from Mo to Cr was observed [95] for thermal CO substitution in $[M(CO)_4(phen)]$. The rate constant of the thermal associative CO substitution in $[M(CO)_4(phen)]$ was correlated with the spectroscopic MLCT energy and a similarity between the transition state of the thermal reaction and the MLCT excited state was suggested [95].

The virtual disappearance of the associative pathway on going from $[W(CO)_4(phen)]$ to $[W(CO)_4(DAB)]$ complexes seems to originate in two interrelated effects: (i) the W→DAB MLCT excited state in DAB complexes is largely delocalized over the W(DAB) chelate ring. This diminishes the charge separation and, hence, the electrophilicity of the W atom in the MLCT excited state. (ii) The excited-state lifetime is very short, as was manifested by the lack of emission of the $[W(CO)_4(DAB)]$ complexes [1,9]. Hence, any type of bimolecular interaction is unlikely for DAB complexes.

The ^{3}MLCT excited states are populated upon visible or near-UV irradiation by intersystem crossing from the optically prepared lowest $^1A_1$ MLCT excited state and higher M→CO or M→diimine MLCT states, respectively [65,69]. Some of the peculiar excitation-wavelength dependences of the quantum-yield of $[M(CO)_4(phen)]$ complexes; M = Mo or W [78,84,85] seem to reflect an excitation-wavelength dependence of the efficiency of intersystem crossing into the ^{3}MLCT states.

Besides associative substitution, ^{3}MLCT excited states of $[W(CO)_4(phen)]$ are also capable of bimolecular electron transfer with *N*,*N*′-dimethyl-4,4′-bipyridinium dication, MV^{2+} [96]. However, the prompt character of this reaction, whereby the reduced $MV^{\bullet+}$ product is formed within 30 ps after excitation, suggests some pre-association between the reactants. Electron transfer from higher and/or vibrationally hot MLCT excited states to the C_2Cl_4 solvent was also postulated [96].

In conclusion, the photochemical reactivity of $[M(CO)_4(\alpha\text{-diimine})]$ complexes can be attributed to dissociative M→CO MLCT states that are populated by UV irradiation, dissociative M→diimine ^{1}MLCT states, populated by visible irradiation, and to non-dissociative ^{3}MLCT states that are populated nonradiatively after either UV or visible irradiation by an excitation-wavelength dependent intersystem crossing from upper excited states. ^{3}MLCT states are capable of associative bimolecular reactions but only if they have sufficiently long lifetime, that is for M = Mo or W, diimine = polypyridine. The different photochemical pathways of $[M(CO)_4(\alpha\text{-diimine})]$ complexes are visualized in Fig. 7.

Further aspects of reactivity of MLCT excited states has been recently reviewed in refs. [91,93].

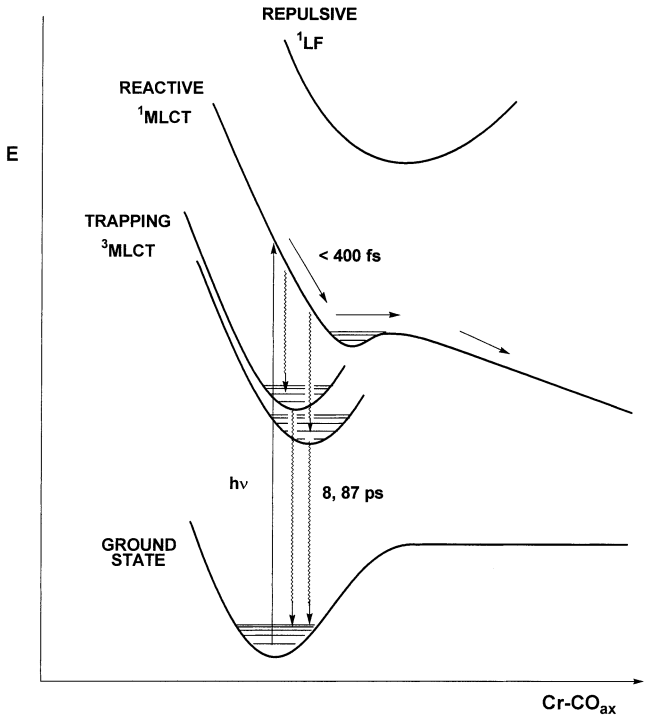

Fig. 8. Excited state dynamics of $[Cr(CO)_4(bpy)]$.

16. Prompt CO dissociation from $[Cr(CO)_4(bpy)]$: ultrafast excited-state dynamics determine photochemical quantum yields

The quantum yield of CO dissociation from $[Cr(CO)_4(bpy)]$ under visible irradiation is less than unity and, moreover, it decreases as the irradiation wavelength increases across the spectral region of the lowest MLCT absorption band [86], see Fig. 9. This excitation-wavelength dependence shows that the reactive state 'keeps the memory' of the initial excitation energy and excludes an occurrence of any relaxation process that would take place between the optical excitation and splitting of the Cr–CO bond. In other words, the excitation-wavelength dependence of the photochemical quantum yield implies that the CO dissociation occurs from higher vibronic levels of the optically prepared b^1A_1 M→bpy MLCT excited state, prior to or in competition with any vibrational or electronic relaxation. This conclusion is in full agreement with femtosecond time-resolved spectra [80], which have demonstrated that CO dissociation from $[Cr(CO)_4(bpy)]$ indeed occurs as an ultrafast evolution on the potential energy surface of the optically populated b^1A_1 M→bpy MLCT excited state, being completed in less than 400 fs (see Fig. 8). Moreover, it was shown [80–82] that two low-lying ^{3}MLCT excited states are populated concomitantly with CO dissociation. These states are unreactive, acting as trapping states with respect to CO dissociation. The initial excited state dynamics of $[Cr(CO)_4(bpy)]$ is thus determined by the ultrafast (<400 fs) branching of the evolution of the optically populated b^1A_1 MLCT state between CO dissociation and relaxation to lower trapping states, as is shown in Fig. 8. The corresponding branching ratio, measured by fs time-resolved spectroscopy [80], depends on the excitation wavelength in the same way as the overall photochemical quantum yield, as can be seen by comparing Figs. 9 and 10. The case study of the $[Cr(CO)_4(bpy)]$ photochemistry [80–82,86] has clearly demonstrated that the early excited state dynamics determine the overall outcome of $[Cr(CO)_4(bpy)]$ photochemistry and that the branching of the evolution of an optically prepared ^{1}MLCT state between Cr–CO bond splitting and relaxation to unreactive states limits the photochemical quantum yield, see Fig. 8. Similar behavior was found for photochemical Re-R bond homolysis in $[Re(R)(CO)_3(dmb)]$ complexes [97] and for CO photodissociation from various $CpM(CO)_n$ complexes, that generates catalytically important species implicated in photochemical C–H bond activation [98–103]. It is suggested that ultrafast branching of excited-state evolution between reactive and unreactive pathways is a general mechanism that limits quantum yields of organometallic photoreactions [91,93,104]. Moreover, detailed studies of the $[Cr(CO)_4(bpy)]$ photochemistry have shown that organometallic photochemistry cannot be interpreted by considering only the orbitals that are depopulated and populated, respectively, by optical excitation. Instead, relative positions and energy ordering of Franck-Condon, dissociative, and unreactive ('trapping') excited states, as well as their interactions and orbital mixing along possible reaction coordinates should be taken into account [91,93]. Interactions between excited states and the ground state can also be important. A close interplay between experiment and theory is essential to understand these processes.

17. Concluding remarks

$[M(CO)_4(\alpha\text{-diimine})]$ (M = Cr, Mo, W) complexes clearly exhibit many interesting features whose detailed investigations have much contributed to our understanding of spectroscopy, electrochemistry and photochemistry of organometallic compounds, which goes far beyond the limited class of these compounds. It can be expected that more detailed studies of $[M(CO)_4(\alpha\text{-diimine})]$ complexes will follow, perhaps using the most advanced and new experimental and theoretical techniques. The role of $[M(CO)_4(\alpha\text{-diimine})]$ complexes as excellent models for studying new physico-chemical phenomena and testing new theories is undisputable. On the other hand, $[M(CO)_4(\alpha\text{-diimine})]$ complexes have never achieved the fame and importance of other diimine complexes such as $[Ru(bpy)_3]^{2+}$, $[Os(bpy)_3]^{2+}$

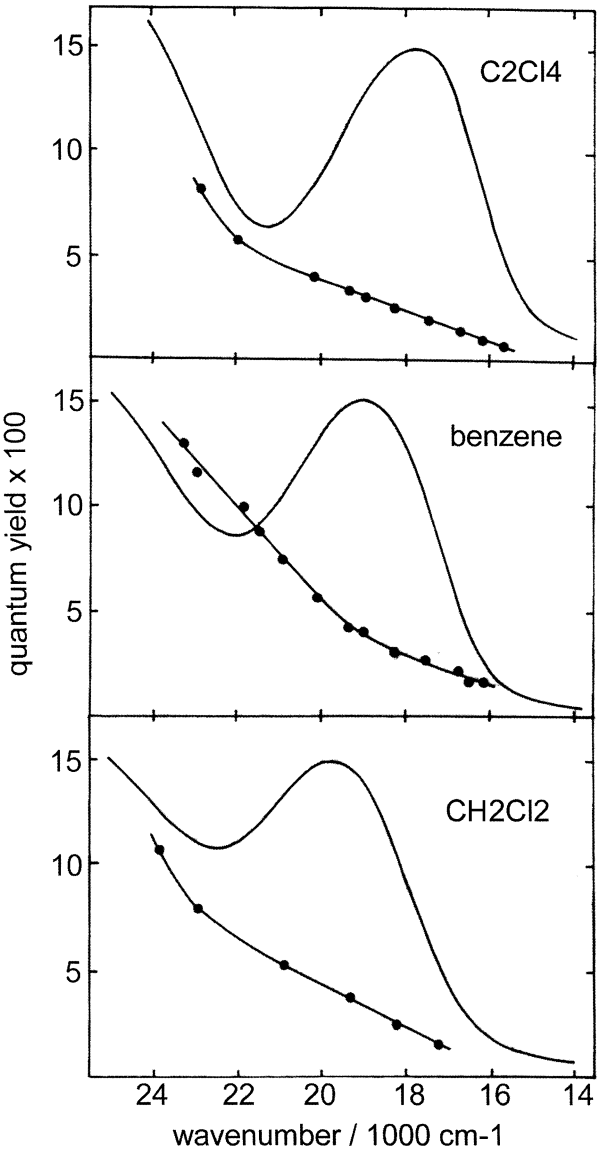

Fig. 9. Excitation-wavelength dependence of quantum yields of dissociative CO substitution in $[Cr(CO)_4(bpy)]$ by PPh_3 in various solvents, displayed together with $[Cr(CO)_4(bpy)]$ absorption spectra [86].

or $[Re(Cl)(CO)_3(bpy)]$. This could be caused by their relatively short excited-state lifetimes, low excited-state energies, lability of the oxidized species and low reactivity of the one-electron reduction products toward substrates. These features are not favorable for the usual applications of photo- and electro-active compounds as photosensitizers, photocatalysts or electrocatalysts. On the other hand, solvatochromism and rigidichromism of MLCT emission is finding a good use in monitoring polymerization reactions and polymer curing [105,106]. Further interesting development is signaled by the recently synthesized $[M(CO)_4$(ferrocenyl-DAB)] complexes which show an electronic interaction between the ferrocenyl units through the $M(CO)_4$(DAB) moiety,

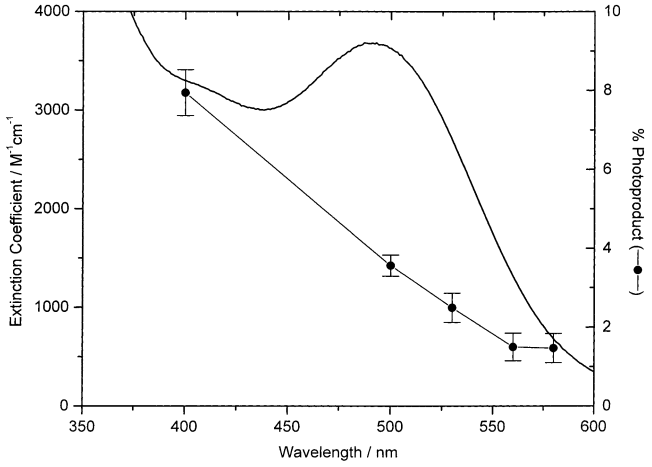

Fig. 10. Excitation-wavelength dependence of the relative contribution of the $[Cr(S)(CO)_3(bpy)]$ primary photoproduct to the transient absorption at 800 nm, extrapolated to the time of optical excitation (●). Measured by femtosecond time-resolved spectroscopy in pyridine [80]. Absorption spectrum of $[Cr(CO)_4(bpy)]$ in pyridine is shown as well.

with interesting spectroscopic and electrochemical consequences [107]. This indicates that new types of behavior can be expected for complexes of DAB ligands which bear functional groups on their N atoms.

Acknowledgements

It is my great pleasure to thank to all my colleagues and friends with whom I have studied various aspects of $[M(CO)_4(\alpha$-diimine)] complexes: Jana Víchová, František Hartl, Stanislav Záliš, Ian R. Farrell, Chantal Daniel, Dominique Guillaumont, Cooper H. Langford, Elspeth Lindsay, Michael W. George, Ian G. Virrels, Jonas Peters, Wolfgang Kaim, Matthias Wanner, Frank Baumann and Friedrich-Wilhelm Grevels. Especially, I thank Dick Stufkens for nearly 20 years of a fruitful scientific collaboration, exciting scientific discussions and ideas on organometallic spectroscopy and photochemistry. This work was carried out as a part of the European collaborative COST project D14/0001/99.

References

[1] D.J. Stufkens, Coord. Chem. Rev. 104 (1990) 39.
[2] L.H. Staal, A. Terpstra, D.J. Stufkens, Inorg. Chim. Acta 34 (1974) 97.
[3] R.W. Balk, D.J. Stufkens, A. Oskam, Inorg. Chim. Acta 28 (1978) 133.
[4] L.H. Staal, D.J. Stufkens, A. Oskam, Inorg. Chim. Acta 26 (1978) 255.
[5] R.W. Balk, D.J. Stufkens, A. Oskam, Inorg. Chim. Acta 34 (1979) 267.

[6] R.W. Balk, T. Snoeck, D.J. Stufkens, A. Oskam, Inorg. Chem. 19 (1980) 3015.
[7] R.W. Balk, D.J. Stufkens, A. Oskam, J. Chem. Soc. Dalton Trans. (1982) 275.
[8] H.K. van Dijk, P.C. Servaas, D.J. Stufkens, A. Oskam, Inorg. Chim. Acta 104 (1985) 179.
[9] P.C. Servaas, H.K. van Dijk, T.L. Snoeck, D.J. Stufkens, A. Oskam, Inorg. Chem. 24 (1985) 4494.
[10] W. Kaim, S. Kohlmann, A.J. Lees, T.L. Snoeck, D.J. Stufkens, M.M. Zulu, Inorg. Chim. Acta 210 (1993) 159.
[11] A. Vlček, Jr., F.-W. Grevels, T.L. Snoeck, D.J. Stufkens, Inorg. Chim. Acta 278 (1998) 83.
[12] D.J. Stufkens, J. Mol. Struct. 79 (1982) 67.
[13] H.K. van Dijk, D.J. Stufkens, A. Oskam, J. Am. Chem. Soc. 111 (1989) 541.
[14] M.W. Kokkes, D.J. Stufkens, A. Oskam, J. Chem. Soc. Dalton Trans. (1983) 439.
[15] J. van Slageren, F. Hartl, D.J. Stufkens, D.M. Martino, H. van Willigen, Coord. Chem. Rev. 208 (2000) 309.
[16] D.J. Stufkens, A. Vlček, Jr., Coord. Chem. Rev. 177 (1998) 127.
[17] D.J. Stufkens, A. Vlček, Jr., The Spectrum 9 (1996) 2.
[18] D.J. Stufkens, M.P. Aarnts, B.D. Rossenaar, A. Vlček, Jr., Pure Appl. Chem. 69 (1997) 831.
[19] D.J. Stufkens, M.P. Aarnts, J. Nijhoff, B.D. Rossenaar, A. Vlček, Jr., Coord. Chem. Rev. 171 (1998) 93.
[20] D.J. Stufkens, Comments Inorg. Chem. 13 (1992) 359.
[21] G.J. Stor, D.J. Stufkens, A. Oskam, Inorg. Chem. 31 (1992) 1318.
[22] H.A. Nieuwenhuis, D.J. Stufkens, A. Oskam, Inorg. Chem. 33 (1994) 3212.
[23] B.D. Rossenaar, C.J. Kleverlaan, M.C.E. van de Ven, D.J. Stufkens, A. Oskam, J. Fraanje, K. Goubitz, J. Organomet. Chem. 493 (1995) 153.
[24] J.W.M. van Outersterp, D.J. Stufkens, J. Fraanje, K. Goubitz, A. Vlček, Jr., Inorg. Chem. 34 (1995) 4756.
[25] B.D. Rossenaar, D.J. Stufkens, A. Vlček, Jr., Inorg. Chem. 35 (1996) 2902.
[26] M.P. Aarnts, D.J. Stufkens, M.P. Wilms, E.J. Baerends, A. Vlček, Jr., I.P. Clark, M.W. George, J.J. Turner, Chem. Eur. J. 2 (1996) 1556.
[27] M.P. Aarnts, D.J. Stufkens, A. Oskam, J. Fraanje, K. Goubitz, Inorg. Chim. Acta 256 (1997) 93.
[28] M.P. Aarnts, M.P. Wilms, D.J. Stufkens, E.J. Baerends, A. Vlček, Jr., Organometallics 16 (1997) 2055.
[29] M.P. Aarnts, A. Oskam, D.J. Stufkens, J. Fraanje, K. Goubitz, N. Veldman, A.L. Spek, J. Organomet. Chem. 531 (1997) 191.
[30] C.J. Kleverlaan, D.J. Stufkens, Inorg. Chim. Acta 284 (1999) 61.
[31] J. van Slageren, D.J. Stufkens, Inorg. Chem. 40 (2001) 277.
[32] M.W. Kokkes, T.L. Snoeck, D.J. Stufkens, A. Oskam, M. Cristophersen, C.H. Stam, J. Mol. Struct. 131 (1985) 11.
[33] J. van Slageren, A. Klein, S. Záliš, D.J. Stufkens, Coord. Chem. Rev. 219–221 (2001) 937.
[34] W. Kaim, Inorg. Chem. 23 (1984) 3365.
[35] S. Ernst, W. Kaim, J. Am. Chem. Soc. 108 (1986) 3578.
[36] W. Kaim, S. Kohlmann, Inorg. Chem. 25 (1986) 3442.
[37] S. Ernst, W. Kaim, Inorg. Chim. Acta 114 (1986) 123.
[38] W. Kaim, S. Kohlmann, Inorg. Chem. 26 (1987) 68.
[39] S. Záliš, C. Daniel, A. Vlček, Jr., J. Chem. Soc. Dalton Trans. (1999) 3081.
[40] I.R. Farrell, F. Hartl, S. Záliš, M. Wanner, W. Kaim, A. Vlček, Jr., Inorg. Chim. Acta 318 (2001) 143.
[41] I.R. Farrell, F. Hartl, S. Záliš, T. Mahabiersing, A. Vlček, Jr., J. Chem. Soc. Dalton Trans. (2000) 4323.
[42] S. Záliš, I.R. Farrell, A. Vlček, Jr., Inorg. Chem., submitted.
[43] H. Jinshuan, C. Qingrong, W. Manfrag, H. Meiyun, Chin. J. Struct. Chem. 4 (1985) 66.
[44] H. Jinshuan, C. Qingrong, W. Manfrag, L. Shimei, Chin. J. Struct. Chem. 4 (1985) 69.
[45] N.S. Magomedova, G.K.-I. Magomedov, Metalloorg. Khim. 3 (1990) 129.
[46] H. tom Dieck, T. Mack, K. Peters, H.-G. von Schnering, Z. Naturforsch. 38b (1983) 568.
[47] W. Majunke, D. Leibfritz, T. Mack, H. tom Dieck, Chem. Ber. 108 (1975) 3025.
[48] H. tom Dieck, K.-D. Franz, F. Hohmann, Chem. Ber. 108 (1975) 163.
[49] D. Miholová, B. Gaš, S. Záliš, J. Klíma, A.A. Vlček, J. Organomet. Chem. 330 (1987) 75.
[50] D. Miholová, A.A. Vlček, J. Organomet. Chem. 279 (1985) 317.
[51] F. Hartl, unpublished results.
[52] J. Hanzlík, L. Pospíšil, A.A. Vlček, M. Krejčík, J. Electroanal. Chem. 331 (1992) 831.
[53] Y. Kaizu, H. Kobayashi, Bull. Chem. Soc. Jpn. 43 (1970) 2492.
[54] Y. Kaizu, H. Kobayashi, Bull. Chem. Soc. Jpn. 45 (1972) 470.
[55] A. Vlček, Jr., F. Baumann, W. Kaim, F.-W. Grevels, F. Hartl, J. Chem. Soc. Dalton Trans. (1998) 215.
[56] W. Kaim, S. Ernst, J. Phys. Chem. 90 (1986) 5010.
[57] B.C. Noble, R.D. Peacock, Spectrochim. Acta 46A (1990) 407.
[58] W. Kaim, J. Am. Chem. Soc. 104 (1982) 3883.
[59] W. Kaim, Coord. Chem. Rev. 76 (1987) 187.
[60] M. Symons, Chemical and Biochemical Aspects of Electron-Spin Resonance Spectroscopy, Van Nostrand Reinhold, Wokingham, UK, 1978.
[61] F. Hartl, A. Vlček, Jr., Inorg. Chem. 35 (1996) 1257.
[62] A.-L. Barra, L.-C. Brunel, F. Baumann, M. Schwach, M. Moscherosch, W. Kaim, J. Chem. Soc. Dalton Trans. (1999) 3855.
[63] H. Saito, J. Fujita, K. Saito, Bull. Chem. Soc. Jpn. 41 (1968) 359.
[64] H. Saito, J. Fujita, K. Saito, Bull. Chem. Soc. Jpn. 41 (1968) 863.
[65] K.A. Rawlins, A.J. Lees, Inorg. Chem. 28 (1989) 2154.
[66] R.S. Panesar, N. Dunwoody, A.J. Lees, Inorg. Chem. 37 (1998) 1648.
[67] D. Guillaumont, C. Daniel, A. Vlček, Jr., Inorg. Chem. 36 (1997) 1684.
[68] D. Guillaumont, C. Daniel, A. Vlček, Jr., J. Phys. Chem. A 105 (2001) 1107.
[69] I.R. Farrell, J. van Slageren, S. Záliš, A. Vlček, Jr., Inorg. Chim. Acta 315 (2001) 44.
[70] D.M. Manuta, A.J. Lees, Inorg. Chem. 25 (1986) 1354.
[71] S. Ernst, Y. Kurth, W. Kaim, J. Organomet. Chem. 302 (1986) 211.
[72] R. bin Ali, J. Burgess, M. Kotowski, R. van Eldik, Transition Met. Chem. 12 (1987) 230.
[73] D.M. Manuta, A.J. Lees, Inorg. Chem. 22 (1983) 3825.
[74] D.M. Manuta, A.J. Lees, Inorg. Chem. 25 (1986) 3212.
[75] W. Kaim, S. Kohlmann, S. Ernst, B. Olbrich-Deussner, C. Bessenbacher, A. Schultz, J. Organomet. Chem. 321 (1987) 215.
[76] D.R. Gamelin, M.W. George, P. Glyn, F.-W. Grevels, F.P.A. Johnson, W. Klotzbucher, S.L. Morrison, G. Russell, K. Schaffner, J.J. Turner, Inorg. Chem. 33 (1994) 3246.
[77] A.J. Lees, Chem. Rev. 87 (1987) 711.
[78] E. Lindsay, A. Vlček, Jr., C.H. Langford, Inorg. Chem. 32 (1993) 2269.
[79] J.-H. Perng, J.I. Zink, Inorg. Chem. 29 (1990) 1158.
[80] I.R. Farrell, P. Matousek, A. Vlček, Jr., J. Am. Chem. Soc. 121 (1999) 5296.
[81] A.J. Vlček, Jr., I.R. Farrell, D.J. Liard, P. Matousek, M. Towrie, A.W. Parker, D.C. Grills, M.W. George, J. Chem. Soc. Dalton Trans. (2002) 701.
[82] I.R. Farrell, P. Matousek, M. Towrie, D.C. Grills, M.W. George, A.J. Vlček, Jr., A.W. Parker, Inorg. Chem., in press.

[83] S. Wieland, K.B. Reddy, R. van Eldik, Organometallics 9 (1990) 1802.
[84] W.-F. Fu, R. van Eldik, Inorg. Chem. 37 (1998) 1044.
[85] W.F. Fu, R. van Eldik, Organometallics 16 (1997) 572.
[86] J. Víchová, F. Hartl, A. Vlček, Jr., J. Am. Chem. Soc. 114 (1992) 10903.
[87] W.F. Fu, R. van Eldik, Inorg. Chim. Acta 251 (1996) 341.
[88] M.S. Wrighton, D.L. Morse, J. Organomet. Chem. 97 (1975) 405.
[89] F.-W. Grevels, K. Kerpen, W. Klotzbücher, K. Schaffner, R. Goddard, B. Weimann, C. Kayran, S. Özkar, Organometallics 20 (2001) 4775.
[90] G.L. Geoffroy, M.S. Wrighton, Organomet. Photochem., Academic Press, New York, 1979.
[91] A. Vlček, Jr., Coord. Chem. Rev. 177 (1998) 219.
[92] I.G. Virrels, M.W. George, J.J. Turner, J. Peters, A. Vlček, Jr., Organometallics 15 (1996) 4089.
[93] I.R. Farrell, A. Vlček, Jr., Coord. Chem. Rev. 208 (2000) 87.
[94] A. Vlček, Jr., J. Víchová, F. Hartl, Coord. Chem. Rev. 132 (1994) 167.
[95] S. Wieland, K.B. Reddy, R. van Eldik, Organometallics 9 (1990) 1802.
[96] E.M. Lindsay, C.H. Langford, A.D. Kirk, Inorg. Chem. 38 (1999) 4771.
[97] I.R. Farrell, P. Matousek, C.J. Kleverlaan, A. Vlček, Jr., Chem. Eur. J. 6 (2000) 1386.
[98] S.E. Bromberg, T. Lian, R.G. Bergman, C.B. Harris, J. Am. Chem. Soc. 118 (1996) 2069.
[99] S.E. Bromberg, H. Yang, M.C. Asplund, T. Lian, B.K. McNamara, K.T. Kotz, J.S. Yeston, M. Wilkens, H. Frei, R.G. Bergman, C.B. Harris, Science 278 (1997) 260.
[100] J.B. Asbury, H.N. Ghosh, J.S. Yeston, R.G. Bergman, T. Lian, Organometallics 17 (1998) 3417.
[101] A.A. Purwoko, A.J. Lees, Inorg. Chem. 34 (1995) 424.
[102] A.A. Purwoko, A.J. Lees, Inorg. Chem. 35 (1996) 675.
[103] N. Dunwoody, A.J. Lees, Organometallics 16 (1997) 5770.
[104] A. Vlček, Jr., Coord. Chem. Rev. 200-202 (2000) 933.
[105] K.A. Rawlins, A.J. Lees, S.J. Fuerniss, K.I. Papathomas, Chem. Mater. 8 (1996) 1540.
[106] A.J. Lees, Coord. Chem. Rev. 177 (1998) 3.
[107] B. Bildstein, M. Malaun, H. Kopacka, M. Fontani, P. Zanello, Inorg. Chim. Acta 300–302 (2000) 16.